10-2001

Derivation of Del180 from sediment core log data' Implications for millennial-scale climate change in the Labrador Sea

M. E. Weber
University of New Brunswick

Larry A. Mayer
University of New Hampshire, larry.mayer@unh.edu

C. Hillaire-Marcel
Universite du Quebec a Montreal

G. Bilodeau
Universite du Quebec a Montreal

F. Rack
Joint Oceanographic Institutions, Inc.

See next page for additional authors

Recommended Citation

Weber, M. E., L. A. Mayer, C. Hillaire-Marcel, G. Bilodeau, F. Rack, R. N. Hiscott, and A. E. Aksu (2001), Derivation of δ18O from sediment core log data: Implications for millennial-scale climate change in the Labrador Sea, Paleoceanography, 16(5), 503–514, doi:10.1029/2000PA000560

PALEOCEANOGRAPHY, VOL. 16, NO. 5, PAGES 503–514, OCTOBER 2001

Derivation of $\delta^{18}O$ from sediment core log data: Implications for millennial-scale climate change in the Labrador Sea

M. E. Weber,[1] L. A. Mayer,[1,2] C. Hillaire-Marcel,[3] G. Bilodeau,[3]
F. Rack,[4] R. N. Hiscott,[5] and A. E. Aksu[5]

Abstract. Sediment core logs from six sediment cores in the Labrador Sea show millennial-scale climate variability during the last glacial by recording all Heinrich events and several major Dansgaard-Oeschger cycles. The same millennial-scale climate change is documented for surface water $\delta^{18}O$ records of *Neogloboquadrina pachyderma* (left coiled); hence the surface water $\delta^{18}O$ record can be derived from sediment core logging by means of multiple linear regression, providing a paleoclimate proxy record at very high temporal resolution (70 years). For the Labrador Sea, sediment core logs contain important information about deepwater current velocities and also reflect the variable input of ice-rafted debris from different sources as inferred from grain-size analysis, the relation of density and *P* wave velocity, and magnetic susceptibility. For the last glacial, faster deepwater currents, which correspond to highs in sediment physical properties, occurred during iceberg discharge and lasted from several centuries to a few millennia. Those enhanced currents might have contributed to increased production of intermediate waters during times of reduced production of North Atlantic Deep Water. Hudson Strait might have acted as a major supplier of detrital carbonate only during lowered sea level (greater ice extent). During coldest atmospheric temperatures over Greenland, deepwater currents increased during iceberg discharge in the Labrador Sea, then surface water freshened shortly thereafter, while the abrupt atmospheric temperature rise happened after a larger time lag of $\geq$1 kyr. The correlation implies a strong link and common forcing for atmosphere, sea surface, and deep water during the last glacial at millennial timescales but decoupling at orbital timescales.

1. Introduction: Climate Variations in the Labrador Sea

The Labrador Sea is an important ocean basin for studying the glacial discharge into the North Atlantic of both the Laurentide and the Greenland ice sheets. It is also important because it is one of the major areas where intermediate waters are renewed by winter mixing [*Lazier*, 1988] and the formation of Labrador Seawater, which extends to ~2 km water depth below the surface mixed layer. Temporal changes in the water mass structure, however, are less well studied for the Labrador Sea than for the open North Atlantic [*Hillaire-Marcel and Bilodeua*, 2000]. The modern (Holocene) circulation is characterized by an anticlockwise gyre of North Atlantic Deep Water (NADW) associated with a strong Western Boundary Undercurrent (>2 km water depth). The major surface currents are the Labrador Current (<1.5 km water depth), which is a near-surface, western boundary current, and the northeast directed Gulf Stream south of the Labrador Sea.

During the last glacial, large volumes of freshwater were released by iceberg calving and subglacial meltwater outflow into the North Atlantic every 7–10 kyr [*Bond et al.*, 1992]. These events perturbated deepwater circulation [*Paillard and Labeyrie*, 1994] and were associated with ice sheet instabilities that gave rise to massive discharge of ice-rafted debris (IRD) into the Labrador Sea and the deposition of detrital carbonate material from the Hudson Strait [*Andrews and Tedesco*, 1992; *Dowdeswell et al.*, 1995]. Icebergs that left the Laurentide ice sheet moved along the Labrador coast and released large quantities of IRD that have been identified as Heinrich events [*Heinrich*, 1988], which are marked by light $\delta^{18}O$ values in planktonic foraminifera [*Bond et al.*, 1992] and low productivity in surface waters [*Hillaire-Marcel et al.*, 1994]. Heinrich events are identified between 40°N and 60°N [*Kissel et al.*, 1999] and may result from internal oscillations of the Laurentide ice sheet [*McAyeal*, 1993]. Intense input glacial freshwater may have led to reduced NADW formation during the events [*Broecker et al.*, 1989]. *Hillaire-Marcel et al.* [1994] reported reduced NADW formation for the Labrador Sea from a stable isotope study that documents a vertically almost homogenous water column during glacials, in contrast to strong stratification during interglacials.

At higher frequencies, millennial-scale air temperature fluctuations over Greenland as recorded in the isotopic signature of air bubbles trapped in the ice sheet [*Dansgaard et al.*, 1993], correspond to changes in the isotopic composition of planktonic foraminifera in North Atlantic glacial sediment [*Bond and Lotti*, 1995]. Accordingly, the atmospheric record and the sea surface record were linked. There is also evidence for a link between atmospheric variability and paleocirculation and possibly to the production of NADW as indicated in sediment physical properties of North Atlantic sediment [*Rasmussen et al.*, 1996; *Moros et al.*, 1997; *Kissel et al.*, 1999]. Here we will use a sediment core log-derived climate proxy to provide evidence that the atmospheric variability over Greenland is linked to both surface water and deepwater variability in Labrador Sea sediment.

[1]Ocean Mapping Group, Department of Geodesy and Geomatics Engineering, University of New Brunswick, Fredericton, New Brunswick, Canada.
[2]Now at Center for Coastal and Ocean Mapping, University of New Hampshire, Durham, New Hampshire, USA.
[3]Center for Research in Isotopic Geochemistry and Geochronology, Université du Quebec à Montréal, Montréal, Quebec, Canada.
[4]Joint Oceanographic Institutions, Inc., Washington, D. C., USA.
[5]Earth Sciences Department, Memorial University of Newfoundland, St. John's, Newfoundland, Canada.

Paper number 2000PA000560.
0883-8305/01/2000PA000560$12.00

2. Climate Proxy Derivation From Sediment Core Logs: Background

Near continuous sediment core logs of physical and optical properties have become substantial and persuasive tools in paleoceanography. Core logs can be gathered rapidly and at millimeter to centimeter resolution. Data quality is improving and currently benefits from of increased attention paid to common calibration and data processing procedures [e.g., *Weber et al.*, 1997; *Best and Dunn*, 1999].

Physical properties are playing an increasingly important role in stratigraphic studies of marine sediment [e.g., *Shackleton et al.*, 1995], with high-resolution timescales being constructed by relating variations of physical properties to variations of, for example, orbital parameters or isotopic reference curves. For longer timescales, deep-sea cores are used as the reference section; for shorter timescales, ice cores are used. Further application includes spectral analyses in order to study the climate response to forcing factors [*Mayer et al.*, 1996]. Underlying this approach is the ability to derive and predict the variation of climatically relevant proxies from sediment core logging since it is the establishment of this relationship that allows the collection of climate proxy data at high resolution [*Mayer*, 1991]. In Pacific biogenic sediment, for instance, carbonate contains the major information about productivity in surface waters and dissolution in deep waters [*Pisias et al.*, 1995]. Therefore a number of successful, sediment core log-based predictions exist for deep-sea carbonate content [e.g., *Mayer*, 1991; *Hagelberg et al.*, 1995; *Weber*, 1998]. Further predictions have been proposed for deep-sea carbonate grain-size distribution [*Mayer et al.*, 1993] and biogenic opal contents [*Weber*, 1998]. For continental margin settings, grain-size distribution [*Weber et al.*, 1997] and magnetite content [*Harris et al.*, 1997] have been derived from sediment core logs.

Here we demonstrate an approach for the derivation of $\delta^{18}O$ values for *Neogloboquadrina pachyderma* (left coiled) during the last glacial cycle from variations of gamma ray density (hereinafter density), compressional wave velocity (hereinafter *P* wave velocity), magnetic susceptibility, and sediment color (gray scale) measured on sediment cores retrieved on the slope off Atlantic Canada. The Labrador Sea cores of this study yield a detailed record of the late Quaternary response of the eastern Laurentide ice sheet to sub-Milankovitch climate forcing. Therefore millennial-scale climate signals such as Heinrich events [*Bond et al.*, 1992] and Dansgaard-Oeschger cycles [*Dansgaard et al.*, 1993] can be identified and studied in great detail by high-resolution physical and optical sediment properties.

In this paper, we will provide evidence that the surface water $\delta^{18}O$ signal and variations recorded in core logs of sediment physical properties are highly correlated for Labrador Sea sediment, implying a strong link that allows the use of sediment core logs as rapid and nondestructive stratigraphic tools for studying millennial-scale climate variability. Furthermore, we will demonstrate that variations recorded in sediment core logs provide important information about current intensities in deep water and that both deepwater and shallow water processes responded to the variable input in the amount of detrital carbonate and IRD. Arguments will be obtained from grain-size analysis, the relation of density and *P* wave velocity, and magnetic susceptibility variations.

3. Material, Methods, and Stratigraphy

The sediment cores presented here were collected and analyzed as part of the Canadian Climate System History and Dynamics Project (CSHD) and the International Marine Global Change Study (IMAGES). Cores were collected in the Labrador Sea (Figure 1) with R/V *Marion Dufresne II* during the first IMAGES cruise MD95 in 1995 with the exception of core MD99-2242, which is from cruise MD99 in 1999. Core locations are given in Table 1. Site MD95-2024 is located off the shelf of Newfoundland on the slope of Orphan Knoll and was taken on the same location as core 91-045-094 studied by *Hillaire-Marcel et al.* [1994]. It spans the last glacial cycle and documents a sequence of eight Heinrich events. Core MD95-2025 is located 75 km to the southwest at Orphan Basin. It is strongly influenced by the Western Boundary Undercurrent and spans the last three glacial cycles, documenting 13 Heinrich events. Cores MD95-2024 and MD95-2025 were both studied in great detail for stable isotopes and geochemistry. Core MD95-2026 is from the northeast flank of the Sackville Spur sediment drift and provides insight into variations in the strength of the Labrador Current. Therefore it was studied for grain-size distribution. Core MD99-2242 is located on the Greenland Rise directly in the path of the Western Boundary Undercurrent and should hence have low interglacial sedimentation rates. Core MD95-2028 is from Fogo Seamount, south of the Grand Banks of Newfoundland, and yields a record of meltwater discharges from the Laurentian Channel over several glacial cycles, whereas core MD95-2029 from the eastern levee of the Laurentian Fan and core MD95-2033 from the Laurentian Margin provide the same record during the Last Glacial Maximum and the following deglaciation. Core MD95-2031 is from the continental slope off Whale Bank, southwest of the Grand Bank, and provides a high-resolution record of deglaciation.

Density, *P* wave velocity, and magnetic susceptibility were determined nondestructively onboard using a MultiSensor Core Logger (Geotek, United Kingdom) at 2-cm increments. This system provides three sensors: a pair of compressional wave transducers to determine the velocity of compressional waves in the core (*P* wave velocity); a gamma ray source and detector to measure the attenuation of gamma rays through the core (density); and a magnetic susceptibility sensor loop to determine the amount of magnetic material present in the sediment. Densities were calculated using varying attenuation coefficients and an iteration procedure described by *Weber et al.* [1997]. In addition, a Minolta chromatometer was used to measure gray scale at 5-cm increments (for method, see *Weber* [1998]). For core MD95-2024, carbonate, stable isotopes, and organic carbon were analyzed at 5-cm increments at Center for Research in Isotopic Geochemistry and Geochronology (GEOTOP), Montreal, using the procedures described by *Hillaire-Marcel et al.* [1994]. For core MD95-2025, stable isotopes and carbonate content were measured at Memorial University of Newfoundland using the procedures described by *Hiscott et al.* [2001]. For core MD95-2026, grain size distribution was determined at Bedford Institute of Oceanography. For the fraction >63 μm, settling tubes were applied, and for the fraction <63 μm, a Sedigraph was used.

Site MD95-2024 is the focus of this study since it contains both a high-resolution stratigraphy and a complete set of sediment core log and sample data at high temporal resolution (70 and 210 years, respectively). The directly determined stratigraphy of this site is based on accelerator mass spectrometry (AMS) ^{14}C dates to ~30 ka, which were measured at core 91-045-094 from the same location [*Hillaire-Marcel et al.*, 1994]. Sites 91-045-094 and MD95-2024 were correlated using $\delta^{18}O$ records from *N. pachyderma* [*Hillaire-Marcel and Bilodeua*, 2000]. For the actual age model we used the high-resolution paleointensity record of *Stoner et al.* [2000], which relies on correlation of site MD95-2024 to the $\delta^{18}O$ record of the Greenland Ice Sheet Project 2 (GISP2) ice core. All sample data from cores 91-045-094 and MD95-2024 are available at the open GEOTOP database (www.geotop.uqam.ca/geotop/paleoceanographicDatabase/eng/database.html). All onboard nondestructive data are available at the IMAGES web site (www.images.cnrs-gif.fr) and a revised version including $\delta^{18}O$ derivations will be made available within the Paleoclimate Data

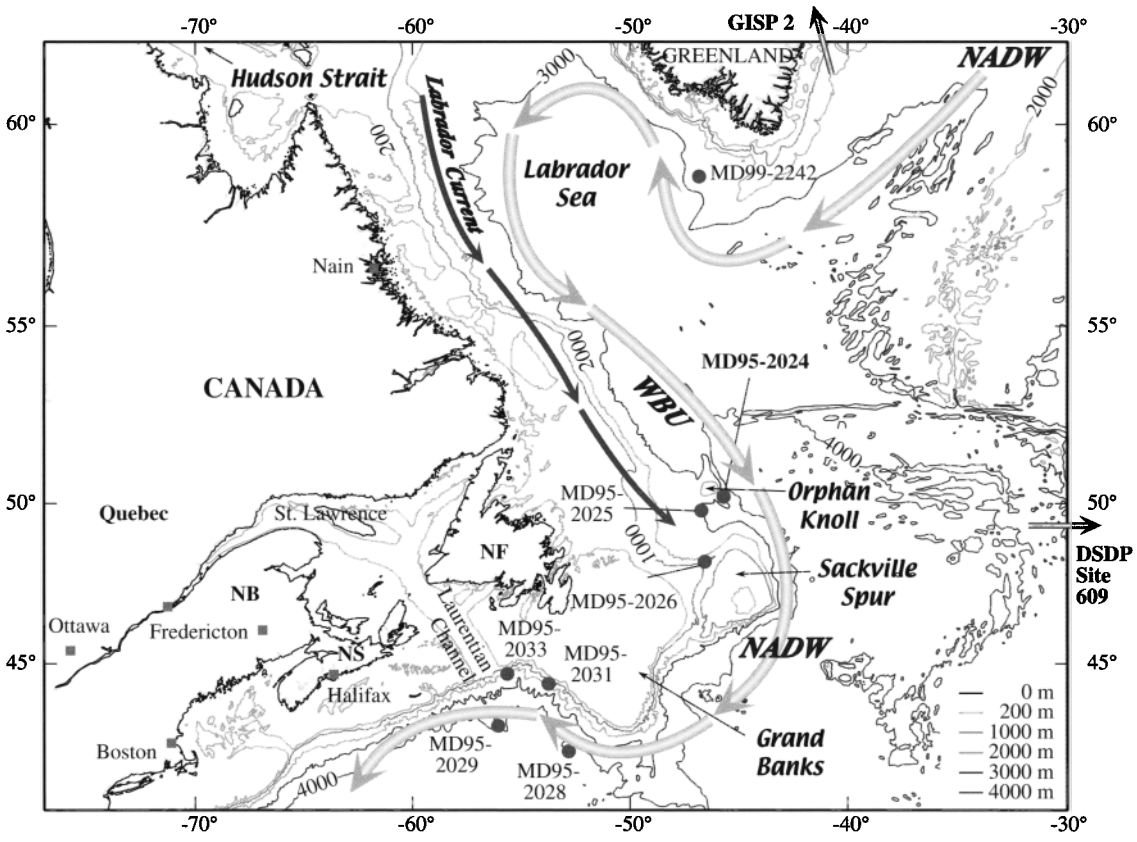

Figure 1. Location map from the Labrador Sea. Cores of this study are from the International Marine Global Change Study (IMAGES) cruise MD95, collected with R/V *Marion Dufresne II* in 1995. Arrow marks the path of North Atlantic Deep Water (NADW) and Labrador Current. Directions for the Greenland Ice Sheet Project 2 (GISP2) ice core and Deep Sea Drilling Program (DSDP) Site 609 are indicated. WBU is Western Boundary Undercurrent; NB is New Brunswick; NS is Nova Scotia; NF is New Foundland.

Network (SEPAN) at the Alfred Wegener Institute for Polar and Marine Research (www.pangaea.de /home/mweber/).

4. The $\delta^{18}O$ Derivation Strategy for Labrador Sea Sediment

Derivation of the surface water $\delta^{18}O$ signal from sediment core logs serves several purposes. First, we are able to gather important paleoceanographic proxy data rapidly, at low costs, and at very high temporal resolution. Second, it helps us to explore the nature of sediment core logs and to understand how these log parameters relate to the planktonic $\delta^{18}O$ signal. This, in turn, enables us to better extract paleoclimate information from sediment core logs, that is, to study the link between surface water processes represented by planktonic $\delta^{18}O$ and sediment core logs.

Reference core MD95-2024 from Orphan Knoll is located at the outlet of the NADW gyre into the open Atlantic (Figure 1). Core MD95-2024 contains marine isotope stages (MIS) 1–5 and thus a detailed record of glacial climate history for the last 120 kyr (Figure 2). Icebergs that left Hudson Strait probably moved south along the Labrador coast before they entered the open North Atlantic. They passed between the continental shelf and Orphan Knoll and released material rich in detrital carbonate and IRD

Table 1. Core Locations[a]

Core	Latitude	Longitude	Water Depth, m	Core Length, m
MD95-2024	50°13′N	45°41′W	3539	29.52
MD95-2025	49°47′N	46°42′W	3009	35.12
MD95-2026	48°14′N	47°40′W	878	27.91
MD95-2028	42°06′N	55°45′W	3368	34.20
MD95-2029	43°07′N	53°16′W	4156	35.10
MD95-2031	44°19′N	53°44′W	1570	27.72
MD95-2033	44°40′N	55°37′W	1412	29.68
MD99-2242	58°55′N	47°07′W	2895	35.36
184KL	6°33′S	90°31′W	4102	12.55
40KL	7°33′N	85°30′W	3810	8.46

[a] MD cores are from the Labrador Sea (cruises MD95 in 1995 and MD99 in 1999), core 184KL is from the eastern equatorial Pacific [*Weber*, 1998], and core 40KL is from the Bay of Bengal [*Weber et al.*, 1997].

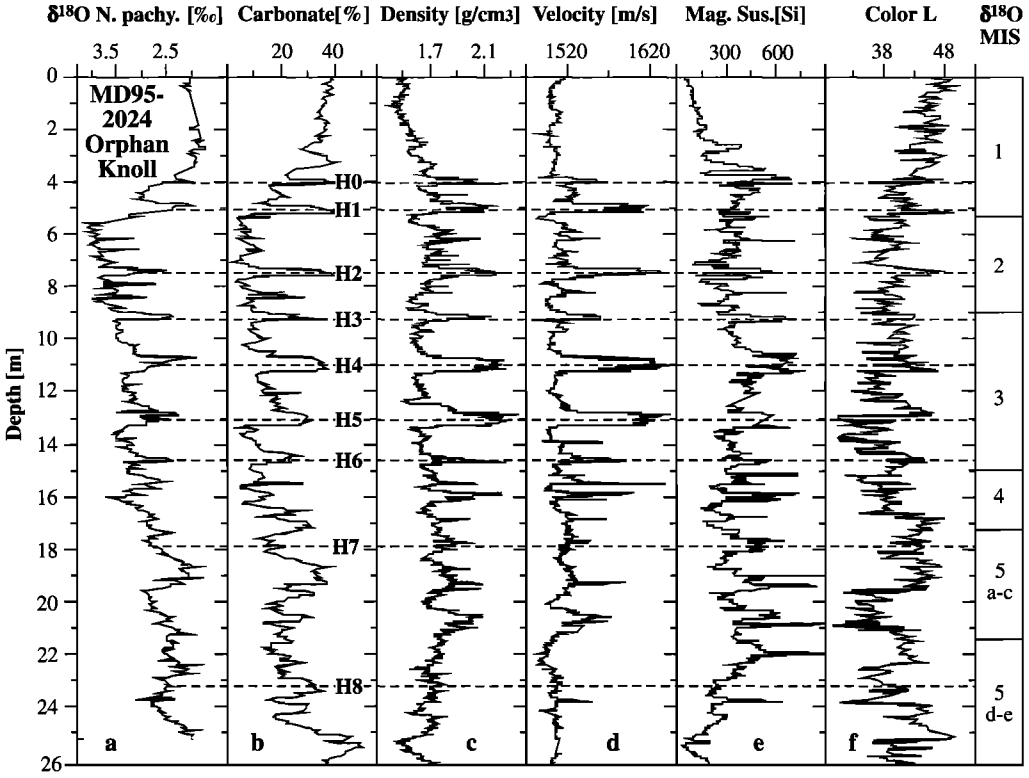

Figure 2. Downcore variations in core MD95-2024. (a) The $\delta^{18}O$ from *N. pachyderma* (left coiled), (b) carbonate content, (c) density, (d) *P* wave velocity, and (e) magnetic susceptibility determined using a MultiSensor Core Logger, and (f) gray scale, determined with a Minolta chromatometer. All records are resampled at 5-cm increments using linear interpolation for derivation purposes shown in Figure 3. H0 through H8 mark Heinrich events. Marine isotopic stages (MIS) are indicated on the right.

while they were melting. Accordingly, Heinrich layers 1–8 are identified at site MD95-2024 as negative peaks in surface water $\delta^{18}O$ values and as maxima in carbonate content, sediment physical properties, and grain size (>125 μm content; Figure 2). We should point out that we measured only bulk carbonate content, but in most cases, the carbonate minerals in the Labrador Sea are ice-rafted limestone and dolostone fragments and the biogenic component (foraminifer shells) is usually very low because of the low glacial productivity in this region. Peaks in bulk carbonate might be related to biogenic carbonate only during some interglacial periods [*Hiscott et al.*, 2001].

All sediment core log parameters for site MD95-2024 correlate in various ways to the $\delta^{18}O$ record of *N. pachyderma* (left coiled). This is indicative of the close relationship among surface water processes (documented by the stable isotope composition) and deepwater processes such as increased current strength and/or increased turbidity current activity (documented by sediment physical properties; see discussion in section 6) and chemical parameters (Figure 2). Light $\delta^{18}O$ values are associated with highs in carbonate, density, *P* wave velocity, magnetic susceptibility, and light colors. Since different parameters were measured at different core depths and at different spatial resolution, we first resampled all data sets at 5-cm increments by linear interpolation in order to achieve a common depth scale.

The comparison reveals that (1) at specific depth intervals (e.g., 5–14 m core depth) the correlation of individual sediment core logs and $\delta^{18}O$ is very good (r is up to 0.9), (2) at short depth intervals below 14 m core depth, correlations are weaker, and (3) sediment core logs and $\delta^{18}O$ are completely out of phase (i.e., they oppose each other) above 5 m core depth. Furthermore, among the core log data sets the correlation with $\delta^{18}O$ varies with depth; that is, at specific depth intervals, $\delta^{18}O$ may correlate very well with one logged property but not necessarily with another one.

Thus, instead of deriving the $\delta^{18}O$ signal in a more conservative way from a single sediment core log, we used multiple linear regression to detect the contribution of individual sediment core log parameters to the overall correlation to the $\delta^{18}O$ signal. This strategy diminishes abrupt offsets of the correlation coefficient, and the derivation still yields reliable results where individual sediment core logs may fail or data gaps may occur.

First, we adjusted all sediment core log records and the $\delta^{18}O$ record to a common variation scale by normalizing them by their variance. This procedure allows a better calculation of the contribution of individual sediment core logs to the derivation and avoids the heavily biased contributions of the original values (e.g., the simple product of density and *P* wave velocity, the acoustic impedance, would reflect 80–95% density variation, depending on lithology). The control of the contribution of individual sediment core logs is recommended when focusing on the study of the physical process that may relate $\delta^{18}O$ and sediment core log, rather than predicting it absolutely from original sediment core log values. Least squares multiple linear regression shows that *P* wave velocity and magnetic susceptibility each contribute ~31% to the correlation, whereas density and gray value provide only ~18% each. We used these proportions to create a stacked record which will be referred to as the "combined" sediment core log. Correlation of the normalized and linearly detrended $\delta^{18}O$ record and the normalized combined sediment core log of site MD95-2024 reveals coefficients from r = 0.9 (5–14 m) to 0 (above 5 m), averaging r = 0.65 (Figure 3e). Only $\delta^{18}O$ values show a linear

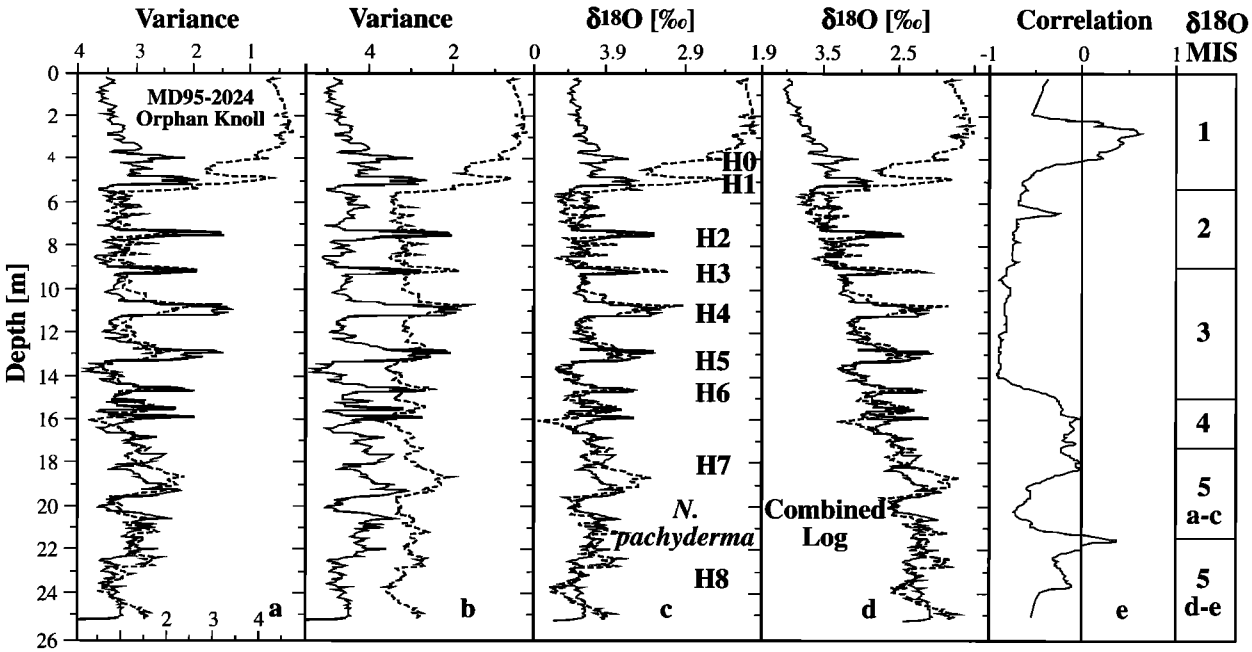

Figure 3. Derivation strategy for $\delta^{18}O$ of *N. pachyderma* in core MD95-2024. Four steps are required to derive the isotopic variation from a combined sediment core log of density, *P* wave velocity, magnetic susceptibility, and gray value. (a) Variance-normalized and linearly detrended $\delta^{18}O$ record of *N. pachyderma* (dashed line) and variance-normalized record of the combined sediment core log (solid line). (b) Combined sediment core log converted to the variance scale of $\delta^{18}O$ of *N. pachyderma* by linear regression. (c) Linear regression used to correlate the combined sediment core log of Figure 3b to the $\delta^{18}O$ record of Figure 3b. (d) Comparison of the combined sediment core log of Figure 3c, corrected for the linear trend of $\delta^{18}O$ and calculated on the true $\delta^{18}O$‰ scale and the original $\delta^{18}O$ record of *N. pachyderm*. (e) Correlation coefficient determined with moving window of 50 data points (2.5 m). The offset of the window from one analysis to another is 1 data point (5 cm). H0 through H8 mark Heinrich events. Marine isotopic stages (MIS) are indicated on the right.

trend (cooling) from isotopic stages 5 though 2 that had to be detrended before the relation between the combined sediment core log and the isotopic record could be explored.

In order to calculate the true $\delta^{18}O$‰ value from the combined sediment core log we calculated a linear regression between the normalized and detrended $\delta^{18}O$ record and the normalized combined sediment core log of Figure 3a, resulting in a common variance scale for both records (Figure 3b). Then a linear regression adjusted the combined sediment core log to the $\delta^{18}O$ variance scale (Figure 3c). In the next step the linear trend was applied to the combined sediment core log, which was then calculated on the true $\delta^{18}O$‰ scale (Figure 3d). Derivations are quite successful with correlation coefficients of up to $r = -0.9$ for many intervals below 5 m core depth, i.e., during the last glacial cycle. Above 5 m core depth, both climate proxy and sediment core log values are decoupled during the Holocene.

In the next step we applied the derivation method to neighboring core MD95-2025, where basically a similar set of isotopic and sediment core log data was obtained [*Hiscott et al.*, 2001]. Site MD95-2025 shows clear indications of Heinrich layers 1–13 (Figure 4) with a core base age of roughly 340 ka. As for the site-specific derivation of the $\delta^{18}O$ signal, both sediment core log and isotopic data of site MD95-2025 were treated with the same set of methods described for core MD95-2024 except that no linear detrending had to be applied to the $\delta^{18}O$ data because that site extends further back in time and comprises several glacials with heavy $\delta^{18}O$ values. The correlation coefficient between $\delta^{18}O$ and combined sediment core log is, on average, lower than that in core MD95-2024 ($r = 0.59$) but is more stable through time. Sites MD95-2024 and MD95-2025 demonstrate that a relationship can be derived between $\delta^{18}O$ values, recorded at the surface mixed layer of the Labrador Sea, and sediment core logs, although the correlation coefficients are not as high as for, for example, carbonate predictions for biogenic open ocean environments.

In order to apply this relationship to the prediction of $\delta^{18}O$ variation from sediment core logging alone, we conducted a second set of experiments. Using site MD95-2024, $\delta^{18}O$ values were obtained directly from original core log values (without scaling to variance) by least squares multiple linear regression. This procedure provides a prediction algorithm that can be applied directly at other sites without further conversion. A comparison of both derivation and prediction methods at site MD95-2025 reveals that, on average, slightly higher correlation coefficients for the site-specific derivation (Figure 4e–g). This is not surprising considering the fact that the site-specific $\delta^{18}O$ data are used to obtain the correlation instead of the MD95-2024 data set. Nonetheless, the independent prediction also yields adequate results for these neighboring locations and thus proves to be a powerful tool to estimate at high resolution the surface water isotopic variation for this part of the Labrador continental margin.

The correlation suggests that the processes affecting the surface of the ocean (as manifested by the variability of planktonic $\delta^{18}O$) and the processes affecting the bottom of the ocean (as expressed by changes in physical properties that responded to variable deep-sea current strength; see discussion in section 6) must have been linked during the last glacial. This link is also indicated by the fact that spectral analysis identifies major Dansgaard-Oeschger frequencies of the GISP2 ice core (1.4–1.5 kyr, 1 kyr, ~0.75 kyr)

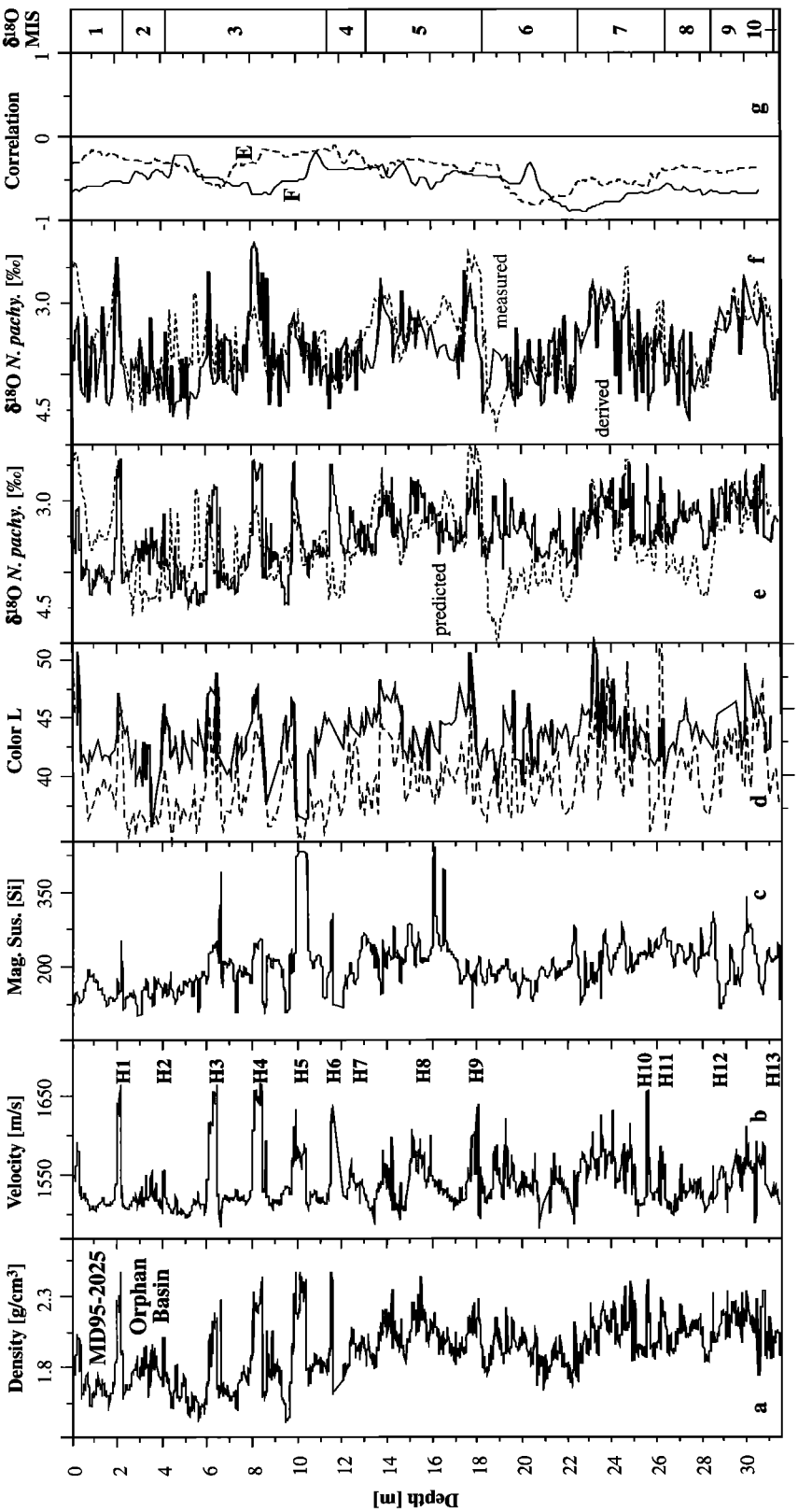

Figure 4. Downcore variations in core MD95-2025. (a) Density, (b) *P* wave velocity, (c) magnetic susceptibility, and (d) gray scale (solid line) and calcium cabonate content (dashed line). (e) The $\delta^{18}O$ variations of *N. pachyderma* (left coiled; dashed line) and the high-resolution prediction of the same record from a combined sediment core log (solid line) of Figures 4a–4c, using equations developed independently for site MD95-2024. (f) The same *N. pachyderma* record (dashed line) and the site-specific $\delta^{18}O$ derivation from a combined sediment core log (solid line) of Figures 4a–4d. For methodology see Figure 3 and refer to text. (g) Correlation coefficient of Figures 4e and 4f as described in Figure 3. H1 through H13 mark Heinrich events. Marine isotopic stages (MIS) are indicated on the right.

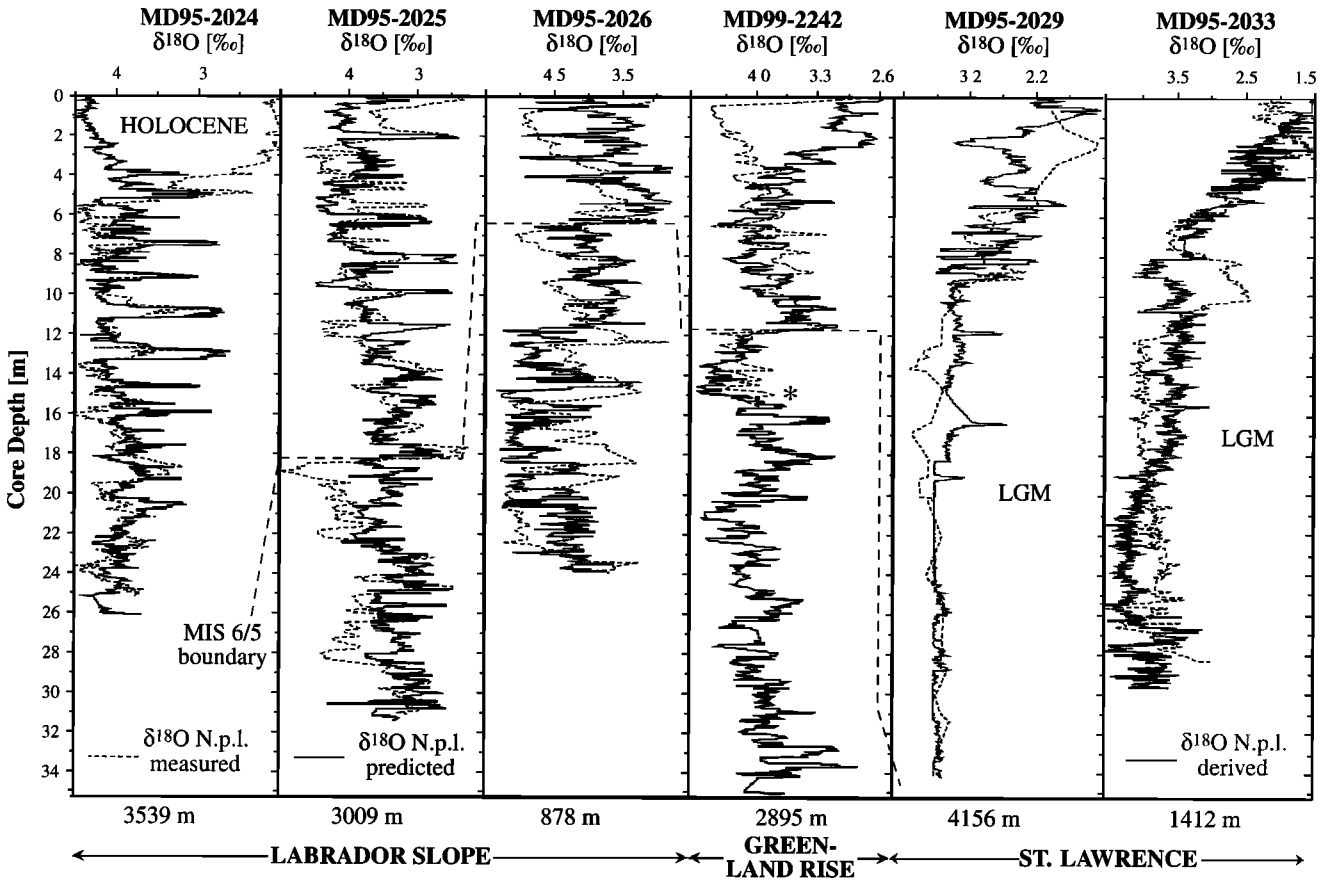

Figure 5. The $\delta^{18}O$ variability of five sites in the Labrador Sea. Shaded curve is $\delta^{18}O$ measured in *N. pachyderma* (left coiled); solid curve is the same $\delta^{18}O$ record predicted from a combined sediment core log using the reference equation developed at site MD95-2024; dashed curve is $\delta^{18}O$ derived site specifically from a combined sediment core log. Note that measured $\delta^{18}O$ record at site MD99-2242 (asterisk) is from twin site 90-013-012P [*Hillaire-Marcel et al.*, 1990], which had to be stretched for depth matching. MIS is marine isotopic stage; LGM is Last Glacial Maximum.

in both sediment core logs and $\delta^{18}O$ values. Also, times when this link was not established are indicated by offsets in the correlation that contain an important climate signal in itself.

Two things should be pointed out. First, the derivation does not capture the huge isotopic amplitude change at MIS boundaries 6/5 and 2/1 which indicates that global signals such as sea level rise (i.e., decrease in global ice volume) affect the surface water isotopic composition to a much greater extent than deepwater processes. Therefore there is strong glacial coupling at millennial timescales between surface-ocean and deep-ocean properties but decoupling at orbital timescales. Second, freshwater peaks in the isotopic record are overpredicted by the log of core MD95-2025 compared to the log of core MD95-2024. The higher amplitude of the deepwater signal at site MD95-2025 (3009 m) points to the proximity to the present high-velocity zone of NADW (2500–3000 m water depth according to *Hillaire-Marcel et al.* [1994]), whereas site MD95-2024 (3539 m) is located 500 m deeper and might have been less affected by velocity variations of major NADW fluctuations.

The next step was to predict or, where necessary, to derive site-specific $\delta^{18}O$ signal for all sites from the Labrador Sea that have the required data sets (cores MD95-2026, MD95-2029, MD95-2033, and MD99-2242; Figure 5). On the Labrador continental slope, all records show the high-amplitude pattern with light $\delta^{18}O$ values corresponding to highs in sediment physical properties as described before. Core MD95-2026 reaches even further back in time (MIS boundary 6/5 is at roughly 6.5 m), and the orbitally induced, large-amplitude variations of the $\delta^{18}O$ signal are not well captured by the physical property-based prediction. Strong millennial-scale variability (although at lower amplitude than at the Labrador continental slope) and coupling of surface- and deep-water proxies is again observed for Greenland Rise core MD99-2242, where the glacial-to-interglacial amplitude is again partially decoupled (e.g., the upper 3 m).

Sites farther south, outside the Labrador Sea at the St. Lawrence outlet, penetrate the last glacial and thus provide a higher-resolution record of oceanic variability. There, oceanic processes must be very different because heavy $\delta^{18}O$ values correspond to highs in sediment physical properties and high-amplitude features are missing for both surface- and deepwater proxies. Consequently, the strong meltwater pulses that affected the surface and deep water in the Labrador Sea did not penetrate that area. Site-specific derivations of the $\delta^{18}O$ signal, which, of course, invert the relation established for Labrador Sea sediment, show that variability is very low during the last glacial for both the $\delta^{18}O$ signal and the combined log; in this respect, both signals are also coupled.

The direct link of surface water proxies such as the isotopic composition of planktonic foraminifera to atmospheric change and ice sheet dynamics is not necessarily given for deepwater proxies such as sediment core log parameters. Since both proxies apparently participated in millennial-scale climate change in the Labrador Sea, a physical link has to exist between the two. To explore

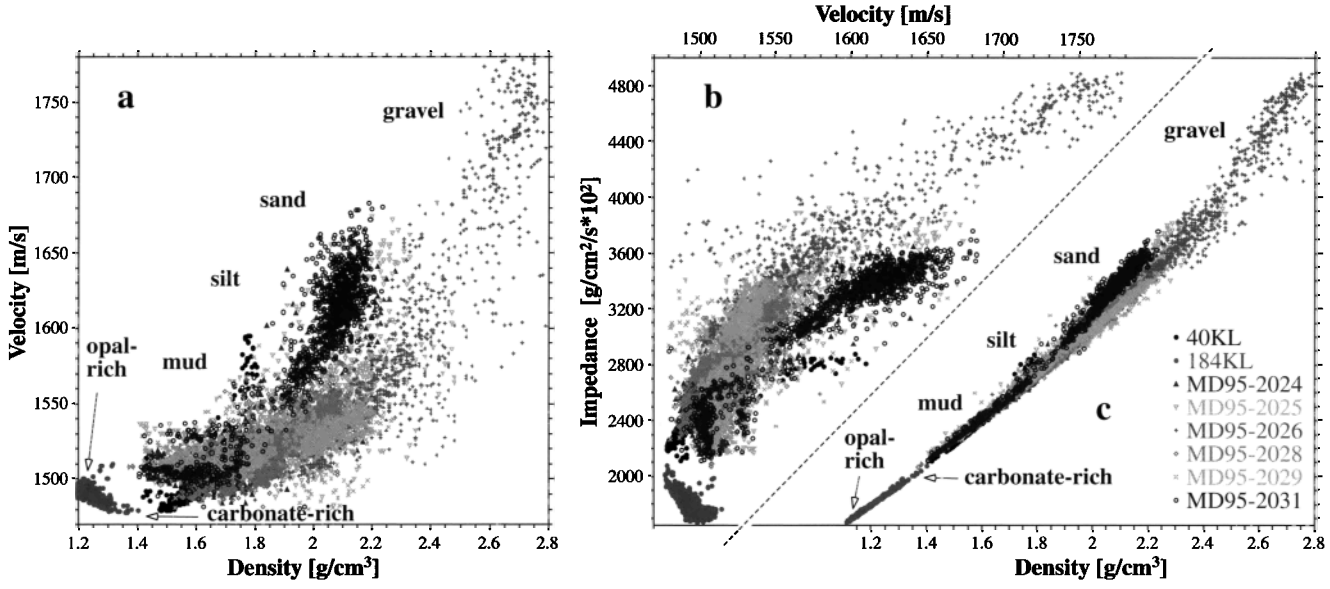

Figure 6. Physical property relations among the CSHD cores MD95-2024, MD95-2025, MD95-2026, MD95-2028, MD95-2029, and MD95-2031 from IMAGES cruise 101 with R/V *Marion Dufresne II*. (a) *P* wave velocity versus density; (b and c) acoustic impedance (the product of density and *P* wave velocity) versus *P* wave velocity and versus density, respectively. For comparison, core 40KL from the Bengal Fan [*Weber et al.*, 1997] and core 184KL from the equatorial Pacific [*Weber*, 1998] are displayed (for location, see Table 1 and Figure 1). Note that physical property relations among sediments containing primarily terrigenous components, provide substantial information about differences in grain size.

the nature of this link, we first studied the relation of sediment core log variation and grain-size distribution.

5. Density and *P* Wave Velocity as Facies Indicator

The relationship between density and *P* wave velocity is one of the most important indirect facies indicators for unconsolidated marine sediment in general [e.g., *Hamilton*, 1970, 1971; *Mienert et al.*, 1988; *Mayer*, 1991; *Weber et al.*, 1997; *Weber*, 1998]. In cores containing predominantly terrigenous material, density increases with *P* wave velocity [*Wood*, 1941]. Here, the relationship is primarily a function of grain-size distribution at relatively high and stable grain densities of 2.5–2.7 g/cm^3 [*Weber et al.*, 1997]. High density ($\geq$2.0 g/cm^3) and high *P* wave velocity ($\geq$1600 m/s) values occur in coarse-grained sediment, where porosity and water content are low. Low density ($\leq$1.6 g/cm^3) and low *P* wave velocity ($\leq$1520 m/s) values occur in fine-grained terrigenous sediment (e.g., from the Bengal Fan, core 40KL, Figure 6), where porosity and water content are higher.

For unconsolidated biogenic sediment (e.g., the southern Atlantic [*Weber et al.*, 1997] and the equatorial Pacific [*Weber*, 1998]), density decreases with increasing *P* wave velocity (core 184KL, Figure 6). This relationship depends on the ratio of biogenic carbonate and opal. *P* wave velocity is high (density is low) in biogenic opal-rich sediment because grain density is low (2.2–2.4 g/cm^3) and intraporosity and rigidity of siliceous skeletons are high [e.g., *Schön*, 1996]. Conversely, *P* wave velocity is low (density is high) in carbonate-rich sediment because grain density is high (2.5–2.8 g/cm^3) and intraporosity and shear resistance of carbonate skeletons are relatively low [*Weber*, 1998]. Hemipelagic sediment shows neither a clear positive nor a clear negative relation of *P* wave velocity and density because they consist primarily of terrigenous material with minor contents of biogenic components.

The trough-shaped *P* wave velocity versus density curve (bottom left of Figure 6a) has a minimum *P* wave velocity of $\sim$1480 m/s, where density ranges from 1.35 to 1.5 g/cm^3. In biogenic settings, *P* wave velocity increases up to 1530 m/s at very low densities of $\sim$1.1 g/cm^3. In terrigenous settings, *P* wave velocity and density may increase up to $\sim$1800 m/s and $\sim$2.8 g/cm^3, respectively, depending on grain size. Values are absolute on a global scale, and thus lithology can be derived indirectly based on this relation. Also, the biogenic and terrigenous end-members of the *P* wave velocity versus density relation allow quantitative assessment of carbonate and opal contents of biogenic environments [*Weber*, 1998] and grain-size distribution in terrigenous environments [*Weber et al.*, 1997] from sediment core logs.

Accordingly, sediments from the Labrador Sea are composed primarily of terrigenous components with minor proportions of biogenic carbonate and opal, and they mainly reflect varying grain sizes (Figure 6c). Using the relationship described in Figure 6, insight into past variations of the current regime and/or the occurrence of IRD may be provided [*McCave et al.*, 1995]. A fine-grained, hemipelagic end-member is present at all sites, whereas a coarse-grained end-member progressively coarsens from cores MD95-2028 and MD95-2029 (relatively fine grained and muddy throughout) to cores MD95-2024, MD95-2031, and MD95-2025 (silty-sandy) and finally to core MD95-2026 (gravelly). Provided that grain size yields relative estimates of current strength, at least if not deposited as IRD, core MD95-2026 would indicate the largest variability in current strength as well as the highest average current velocities. Of course, this is an over-simplification since core MD95-2026 contains gravel as a source signal, which indicates that iceberg activity and deposition is important, too. Grain-size distribution is, in part, a function of water depth with finer sediment at greater water depth and lower current velocities. Accordingly, the shallowest site MD95-2026 at 826 m water depth has the largest variation in grain size and is thus

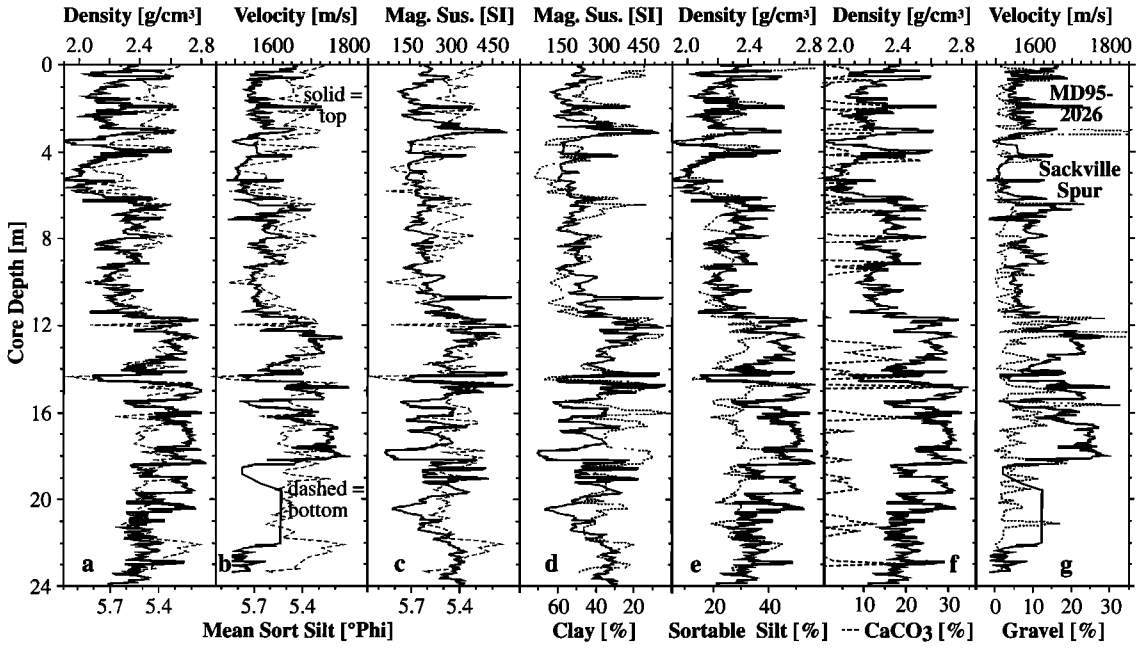

Figure 7. Downcore variations in core MD95-2026. Solid curves (for legend, see top axis) are sediment core log measurements; dashed lines are grain-size parameters (for legend, see bottom axis) and carbonate content. Note that the mean grain size of the sortable silt fraction (Figures 7a–7c) and clay content (Figure 7d) are well correlated to sediment core logs, whereas silt content (Figure 7e) and, especially, carbonate content (Figure 7f) and gravel content (Figure 7g) show no or only weak correlation to sediment core logss.

the logical choice to explore the relationship of grain size and sediment core log data in detail (Figure 7).

6. Possible Link of Surface- and Deepwater Processes

Core MD95-2026 is from Sackville Spur, a sediment drift that is located in intermediate waters. The age control for the younger part is rather limited since there is only one date at 6 m core depth (52 ka), which is beyond the reliability of the ^{14}C method. However, on the basis of the isotopic record (Figure 5), the MIS boundary 6/5 is at roughly 6.5 m core depth. One important grain-size parameter is the mean grain size (given in ^{0}Phi) of the size fraction "sortable silt" (63-10 μm) which reflects most confidently the current strength with stronger currents associated with coarser sizes (lower Φ values) [*McCave et al.*, 1995]. In core MD95-2026, coarser mean grain sizes of the sortable silt fraction are clearly associated with higher densities, velocities, and magnetic susceptibilities (Figures 7a–7c); that is, physical properties at site MD95-2026 clearly trace variations in current strength faster currents at higher values. Neither gravel nor detrital carbonate content, both of which contain direct information about the source and amount of material released by icebergs, correlates in detail to the sediment core log measurements (Figures 7e and 7f). This is a further indication that sediment core log signals are governed by current activity rather than by iceberg activity. Faster deepwater currents during times of increased iceberg discharge argue for either enhanced turbidity current activity or enhanced production of Labrador Seawater.

Highs in physical properties that correspond to times of faster currents at site MD95-2026 are associated with freshening of surface water at neighboring deepwater sites MD95-2024 (Figure 8) and MD95-2025. Although grain size was not studied in detail at core MD95-2024, it is possible that during iceberg discharge, most significantly during Heinrich events, current velocities were increased not only in the Labrador Current but also in the Western Boundary Undercurrent or, alternatively, that the Labrador Current deepened with increased production of Labrador Seawater. The latter possibility is also indicated by the isotopic study of foraminifer assemblages by *Hillaire-Marcel and Bilodeua* [2000]. They show that glacial periods generally have reduced production of intermediate waters, and the Holocene as well as the short interstadials which follow Heinrich events and the successive freshening of surface waters show enhanced production of intermediate waters, comparable to the present-day situation.

As for the timing of events, we should point out that according to the high-resolution paleointensity stratigraphy of *Stoner et al.* [2000] for site MD95-2024 (Figure 8), magnetic susceptibility and detrital carbonate peaks, which are associated with most Heinrich events, match peak cold times in the GISP2 ice core record. At site MD95-2024, sediment physical properties vary in phase, whereas surface water $\delta^{18}O$ lags slightly behind. Coherency is established between the two proxies at various millennial frequencies, indicating a 10°–40° phase shift that translates into, e.g., 70–230 year lag time for surface water $\delta^{18}O$ relative to sediment core log for the major Dansgaard-Oeschger period of 1500 years. Thus, during coldest atmospheric temperatures over Greenland, deepwater currents increased during iceberg discharge in the Labrador Sea, then surface water freshened shortly after, while the abrupt atmospheric temperature rise, which introduced the next interstadial over Greenland, occurred after a larger time lag of $\geq$1 kyr.

Whether or not increased deepwater currents in the Labrador Sea during peak cold times (mainly, Heinrich events) and into the following interstadial interval might have been linked to enhanced production of NADW is unclear. *Oppo and Lehman* [1995] showed that the production of NADW has generally been reduced during the last glacial. At the Faeroe Margin, a strategic site for monitoring the production of NADW, peak cold times showed reduced NADW and increased intermediate water influence on faunal

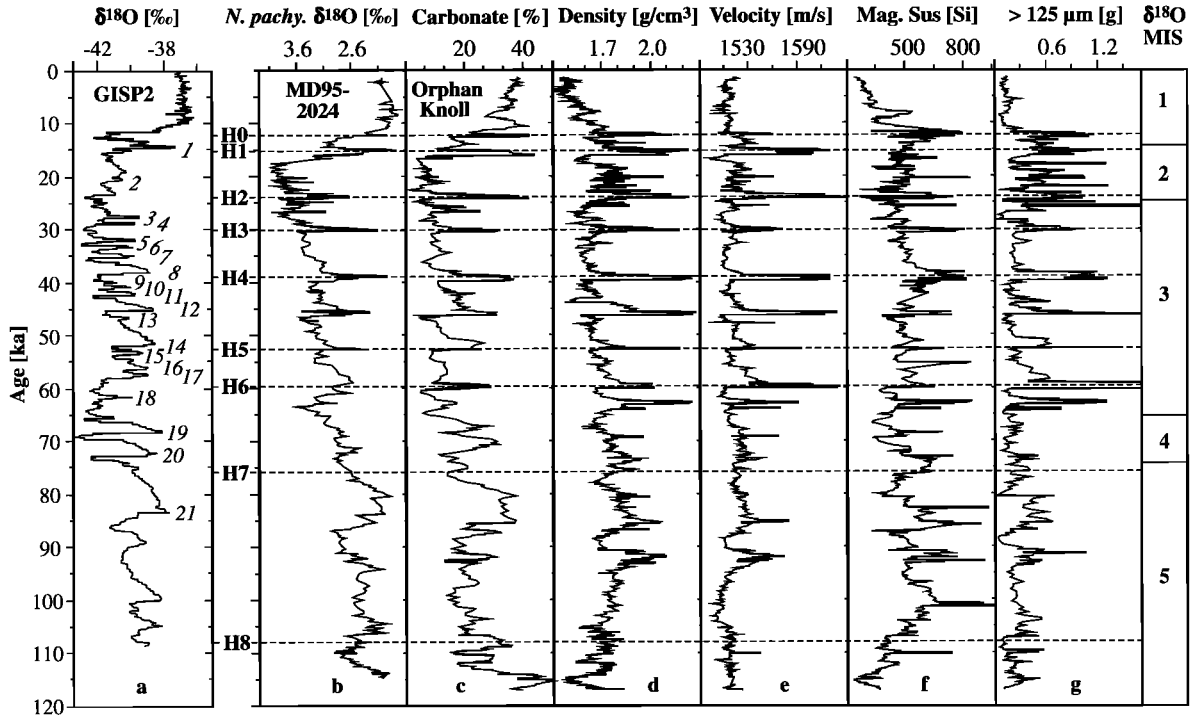

Figure 8. Record of millennial-scale climate change during the last glacial cycle, determined at the summit of Greenland (GISP2 ice core, Figure 8a [*Grootes et al.*, 1993]) and in the Labrador Sea (core MD95-2024, Figures 8b–8h). (a) The $\delta^{18}O$ of air bubbles trapped in ice, (b) density, (c) *P* wave velocity, (d) magnetic susceptibility, (e) $\delta^{18}O$ of *N. pachyderma* (left coiled), (f) carbonate content, and (g) amount of sand >125 µm. H1 through H8 mark Heinrich events. Italic numbers in Figure 8a mark Dansgaard-Oeschger cycles. Marine isotopic stages (MIS) are indicated on the right.

assemblages [*Rasmussen et al.*, 1996]. Therefore the contribution of the Labrador Sea to the formation of intermediate waters seems more likely. Labrador Seawater is currently transported from its formation region in the south central Labrador Sea, to the east, where it becomes stratified and finally involved in convective mixing in the Irminger Basin as part of the formation of NADW [e.g., *Sy et al.*, 1997]. An eastern transport path has to be assumed for the last glacial as well because intensified deepwater currents are not documented for the sites south of the Labrador Sea (cores MD95-2029 and MD95-2033).

For the Labrador Sea, further evidence for increased deepwater currents during freshwater injection into surface waters is provided by magnetic susceptibility, which mainly describes the amount of magnetite in sediments [*Stoner et al.*, 1996]. If neither the source of sediment supply nor the current intensity in deep water changes, magnetic susceptibility should be higher in fine-grained sediment because magnetite is usually concentrated in the very fine silt and clay fractions. In core MD95-2026, magnetic susceptibility and clay content are inversely correlated (Figure 7d). Thus changing source areas with high (e.g., basaltic rocks, volcanic regions) and low (sedimentary basins) amounts of magnetite and/or variations in current intensity caused variations in the signal.

Kissel et al. [1999] studied magnetic susceptibility in a variety of cores that trace the path of NADW between the Nordic Sea and the Bermuda Rise. They concluded that varying magnetic inputs determine the signal, i.e., basaltic material (higher susceptibility) prevailed during interstadials, while continental material (lower susceptibility) dominated during stadials and Heinrich events. Thus periodic changes in the efficiency of transport should explain changes in the relative amount of magnetic material with stronger bottom currents during interstadials and weaker bottom currents during stadials and Heinrich events. Although Labrador Sea sites were not included in their study, their findings would argue against an impact of increased deepwater currents during Heinrich events on the production of NADW; instead, there would be indirect evidence that the intermediate water production was enhanced.

Detrital carbonate and magnetic susceptibility show negative correlation for many North Atlantic sites [*Kissel et al.*, 1999; *Rasmussen et al.*, 1996], including some sites from the Labrador Sea reported by *Andrews and Tedesco* [1992]. This also means that Heinrich layers are low in magnetite [e.g., *Moros et al.*, 1997], partly because of simple dilution by detrital carbonate and partly because the IRD carried a low-magnetite signal. However, most sites used in our study show a positive and in-phase correlation of detrital carbonate and magnetic susceptibility (e.g., Figure 2), pointing to an additional source signal. Detrital carbonate-rich bedrock is located at Hudson Strait [*Andrews and Tedesco*, 1992], whereas siliciclastic bedrock that is richer in magnetite, e.g., gneisses, is located at the coastal Labrador Sea and at Baffin Bay [*Hiscott et al.*, 2001]. Interestingly, Heinrich layers 8 and 7, both of which were deposited at higher sea level at site MD95-2024 (Figure 8), are low in detrital carbonate, whereas younger Heinrich events are associated with distinct peaks in detrital carbonate. Therefore ice dynamics incorporating Hudson Strait as a major sediment supplier might have only operated at lower sea level (greater ice extent). This interpretation is corroborated by site MD95-2025, which covers three glacial cycles. There, Heinrich layers 9, 10, and 12, all of which were deposited at higher sea level, are also low in detrital carbonate (Figure 4), whereas the Heinrich layers of glacial MIS 6 [see *Hiscott et al.*, 2001] are high in detrital carbonate.

Hillaire-Marcel et al. [1994] reported that layers rich in detrital carbonate are, in part, decoupled from IRD deposition. *Stoner et al.* [1996] noted that the correspondence of detrital carbonate content with increased grain size of well-sorted magnetite, but not with coarse fraction, precludes ice rafting as the primary depositional mechanism. They proposed that the ice advances that produced the IRD in the twin core of MD95-2024 (site 91-045-094) also triggered turbiditic flows down the North Atlantic Mid-Ocean Channel (NAMOC), where material rich in detrital carbonate was transported and subsequently deposited at site MD95-2024 from suspension clouds. Therefore one possible link of surface water and deepwater variability would be ice sheet advance, triggering turbidity currents in the deep ocean and meltwater injection into the surface ocean. However, the fact that the deposition of these layers took 0.3–1.3 kyr, based on excess ^{230}Th [*Francois and Bacon*, 1994] and AMS ^{14}C data [*Hillaire-Marcel et al.*, 1994], favors continuing deep-sea currents rather than a distinct event as transport mechanism. Also, the shapes of density and *P* wave velocity curves, which provide a grain-size proxy (see section 5), do not resemble typical turbidites with a coarser-grained lag followed by a fining upward bed; instead, a variety of shapes is observed from plateau-like highs to symmetrical peaks and fining upward beds. Therefore our conclusion is that times of increased iceberg discharge led to increased deepwater currents that continued over hundreds of years to millennia, most likely as contour-following currents along the western Labrador slope.

Figure 8 shows that variations in the glacial surface water isotopic composition in the Labrador Sea were linked to atmospheric processes documented in Greenland ice on millennial timescales. It also shows that deepwater current velocities are linked to freshwater pulses during peak cold times. Thus deepwater variability is also linked to atmospheric variability. This implies that all three parts of the climate system corresponded to the same sub-Milankovitch climate forcing during the last glacial. The nature of this forcing is as yet unknown, and further research will have to be conducted in a variety of fields in order to unravel it.

7. Summary and Conclusions

Records of surface water isotopic composition in the Labrador Sea show millennial-scale climate change signals during the last glacial cycle, all Heinrich events, and several major Dansgaard-Oeschger cycles. The same millennial-scale climate change is documented for deepwater processes by peaks in physical and optical sediment properties that mainly correspond to changes in sediment composition. Heinrich events are marked by light $\delta^{18}O$ values of *N. pachyderma* and highs in density, *P* wave velocity, and magnetic susceptibility. Thus either the variation of surface $\delta^{18}O$ values can be predicted from sediment core logging using the procedure developed at site MD95-2024, or it can be derived by incorporating site-specific $\delta^{18}O$ measurements as shown for site MD95-2025. Both prediction and derivation provide a paleoclimate proxy record at very high temporal resolution (several decades).

For the Labrador Sea, sediment core logs contain important information about deepwater current velocities and also reflect the variable input of IRD from different sources as inferred from grain-size analysis, benthic $\delta^{18}O$, the relation of density and *P* wave velocity, and magnetic susceptibility. The grain-size distribution shows that highs in physical properties correspond to coarser mean grain sizes in the sortable silt fraction, a clear indication of faster deepwater currents. During coldest atmospheric temperatures over Greenland, deepwater currents increased during iceberg discharge in the Labrador Sea, then surface water freshened shortly thereafter. The abrupt atmospheric temperature rise over Greenland, which is associated with the beginning of an interstadial, happened after a larger time lag of $\geq$1 kyr. The correlation implies a strong link and common forcing for atmosphere, sea surface, and deep water for the last glacial at millennial timescales. Times of noncorrelation between sediment core log and surface water $\delta^{18}O$ occur on orbital timescales and contain a climate signal of decoupling of forcing factors; for example, during times of substantial sea level rise, surface water $\delta^{18}O$ values changed dramatically, whereas deepwater properties did not.

Contrary to many North Atlantic sites, Labrador Sea Heinrich events usually show high magnetic susceptibility associated with high detrital carbonate content, pointing to different sources and transport mechanisms. Heinrich layers deposited at higher sea level are relatively low in detrital carbonate, whereas those Heinrich layers deposited at lower sea level are associated with distinct peaks in detrital carbonate. Therefore Hudson Strait, as a major sediment supplier, might have only been active at lower sea level (greater ice extent). The correspondence of detrital carbonate with increased grain size of well-sorted magnetite but not with the coarse fraction precludes ice rafting as the primary depositional mechanism. Instead, enhanced bottom currents that may have lasted several hundred years to a few millennia are associated with Heinrich events.

Variations in current strength along the west coast of the Labrador Sea should be associated with the production of NADW because most of the sites investigated are located within the present-day strong Western Boundary Undercurrent. The fact that we infer faster deepwater currents during coldest air temperatures over Greenland seems to contradict observations that at least during the stadials of the last glacial period, NADW production should have been reduced. However, there are several lines of evidence that increased current strength might have been associated with increased production of intermediate waters in the Labrador Sea.

Acknowledgments. We wish to thank the reviewers M. Lyle, J. Mienert, and C. Kissel for their helpful suggestions and comments. We are also grateful to David Piper for providing grain-size data from core MD95-2026. This study is a contribution to the Climate System History and Dynamics project (CSHD), supported by the National Science and Engineering Research Council of Canada (NSERC). M.E.W. received additional support from the Deutsche Forschungsgemeinschaft (DFG; grant We 2039/2-1).

References

Andrews, J. T., and K. Tedesco, Detrital carbonate-rich sediments, northwest Labrador Sea: Implications for ice-sheet dynamics and iceberg rafting Heinrich events in the North Atlantic, *Geology*, *20*, 1087–1090, 1992.

Best, A. I., and D. E. Dunn, Calibration of marine sediment core loggers for quantitative acoustic impedance studies, *Mar. Geol.*, *160*, 137–146, 1999.

Bond, G., Evidence for massive discharges of icebergs into the North Atlantic Ocean during the last glacial period, *Nature*, *360*, 245–249, 1992.

Bond, G. C., and R. Lotti, Iceberg discharges into the North Atlantic on millennial time scales during the last glaciation, *Science*, *267*, 1005–1010, 1995.

Broecker, W. S., J. P. Kennett, B. P. Flower, J. T. Teller, S. Trumbore, G. Bonani, and W. Woelfli, Routing of meltwater from the Laurentide ice sheet during the Younger Dryas cold episode, *Nature*, *34*, 318–321, 1989.

Dansgaard, W., Evidence for general instability of past climate from a 250 kyr ice core record, *Nature*, *364*, 218–220, 1993.

Dowdeswell, J. A., M. A. Maslin, J. T. Andrews, and I. N. McCave, Iceberg production, debris rafting, and the extend and thickness of Heinrich layers (H1, H2) in North Atlantic sediments, *Geology*, *23*, 301–304, 1995.

Francois, R., and M. P. Bacon, Heinrich events in the North Atlantic: Radiochemical evidence, *Deep Sea Res, Part I, 41*, 315–334, 1994.

Grootes, P. M., M. Stuiver, J. W. C. White, S. Johnsen, and J. Jouzel, Comparison of oxygen isotope records from the GISP2 and GRIP Greenland ice cores, *Nature, 366*, 552–554, 1993.

Hagelberg, T. K., N. G. Pisias, L. A. Mayer, N. J. Shackleton, and A. C. Mix, Spatial and temporal variability of late Neogene equatorial Pacific carbonate: Leg 138, *Proc. Ocean Drill. Program Sci. Results, 138*, 321–336, 1995.

Hamilton, E. L., Sound velocity and related properties of marine sediments, North Pacific, North Pacific, *J. Geophys. Res., 75*, 4423–4447, 1970.

Hamilton, E. L., Prediction of in-situ acoustic and elastic properties of marine sediments, *Geophysics, 36*, 266–284, 1971.

Harris, S. E., A. C. Mix, and T. King, Biogenic and terrigenous sedimentation at Ceara Rise, western tropical Atlantic, supports Pliocene-Pleistocene deepwater linkage between hemispheres, *Proc. Ocean Drill. Program Sci. Results, 154*, 331–345, 1997.

Heinrich, H., Origin and consequences of cyclic ice rafting in the northeast Atlantic Ocean during the past 130,000 years, *Quat Res., 29*, 142–152, 1988.

Hillaire-Marcel, C., and G. Bilodeua, Instabilities in the Labrador Sea water mass structure during the last climatic cycle, *Can. J. Earth Sci., 37*, 795–809, 2000.

Hillaire-Marcel, C., A. Rochon and On-board Participants, The Labrador Sea, CSS-*Hudson* cruise 90-013 report and onboard studies, open file report, Bedford Inst. of Oceanogr., Dartmouth, N. S., Canada, 1990.

Hillaire-Marcel, C., A. de Vernal, G. Bilodeau, and G. Wu, Isotope stratigraphy, sedimentation rates, deep circulation, and carbonate events in the Labrador Sea during the last ~200 ka, *Can. J. Earth Sci., 31*, 63–89, 1994.

Hiscott, R. N., E. A. Aksu, P. Mudie, and D. F. Parsons, A 340,000 year record of ice rafting, palaeoclimatic fluctuations, and shelf-crossing glacial advances in the southwestern Labrador Sea, *Global Planet. Change, 28*, 227–240, 2001.

Holler, P., Geotechnical properties of Antarctic deep sea sediments, *Meteor Forschungsergeb., Reihe C, 39*, 23–36, 1985.

Kissel, C., C. Laj, L. Labeyrie, T. Dokken, A. Voelker, and D. Blamart, Rapid climatic variations during marine isotopic stage 3: Magnetic analysis of sediments from Nordic Seas and North Atlantic, *Earth Planet Sci Lett., 171*, 489–502, 1999.

Lazier, J. R., Temperature and salinity changes in the deep Labrador Sea 1962-1986, *Deep Sea Res., Part I, 35*, 1247–1253, 1988.

Mayer, L. A., Extraction of high-resolution carbonate data for palaeoclimate reconstruction, *Nature, 352*, 148–150, 1991.

Mayer, L. A., E. Jansen, J. Backman, and T. Takayama, Climatic cyclicity at Site 806: The GRAPE record, *Proc. Ocean Drill. Program Sci. Results, 130*, 623–639, 1993.

Mayer, L. A., C. Gobrecht, and N. G. Pisias, Three-dimensional visualization of orbital forcing and climatic response: Interactively exploring the pacemaker of the ice ages, *Geol. Rundsch., 85*, 505–512, 1996.

McAyeal, D. R., Binge/purge oscillations of the Laurentide ice sheet as a cause of North Atlantic's Heinrich events, *Paleoceanography, 8*, 775–784, 1993.

McCave, I. N., B. Manighetti, and S. G. Robinson, Sortable silt and fine sediment size/composition slicing: Parameters for paleocurrent speed and paleoceanography, *Paleoceanography, 10*, 593–610, 1995.

Mienert, J., W. B. Curry, and M. Sarnthein, Sonostratigraphic records from equatorial Atlantic deep-sea carbonates: Paleoceanographic and climatic relationships, *Mar. Geol., 83*, 9–20, 1988.

Moros, M., R. Endler, K. S. Lackschewitz, H. J. Wallrabe-Adams, J. Mienert, and W. Lemke, Physical properties of Reykjanes Ridge sediments and their linkage to high resolution Greenland Ice Sheet Project 2 ice core data, *Paleoceanography, 12*, 687–695, 1997.

Oppo, D. W., and S. J. Lehman, Suborbital timescale variability of North Atlantic Deep Water during the past 200,000 years, *Paleoceanography, 10*, 901–910, 1995.

Paillard, D., and L. Labeyrie, Role of the thermohaline circulation in the abrupt warming after the Heinrich events, *Nature, 372*, 162–164, 1994.

Pisias, N. G., L. A. Mayer, T. R. Janecek, A. Palmer-Julson, and T. H. von Andel, *Proceedings of the Ocean Drilling Program, Scientific Results*, vol. 138, 960 pp., Ocean Drill. Program, College Station, Tex., 1995.

Rasmussen, T. L., E. Thomsen, T. C. E. van Weering, and L. Labeyrie, Rapid changes in surface and deep water conditions at the Faeroe Margin during the last 58,000 years, *Paleoceanography, 11*, 757–771, 1996.

Schön, J. H., *Physical Properties of Rocks: Fundamentals and Principles of Petrophysics*, 583 pp., Pergamon, New York, 1996.

Shackleton, N. J., S. Crowhurst, T. Hagelberg, N. G. Pisias, and D. A. Schneider, A new late Neogene time scale: Application to Leg 138 sites, *Proc. Ocean Drill. Program Sci Results, 138*, 289–319, 1995.

Stoner, J. S., J. E. T. Channell, and C. Hillaire-Marcel, The magnetic signature of rapidly deposited detrital layers from the deep Labrador Sea: Relationship to North Atlantic Heinrich layers, *Paleoceanography, 11*, 309–325, 1996.

Stoner, J. S., J. E. T. Channell, C. Hillaire-Marcel, and C. Kissel, Geomagnetic paleointensity and environmental record from Labrador Sea core MD95-2024: Global marine sediment ice core chronostratigraphy for the last 110 kyr, *Earth Planet. Sci Lett., 183*, 161–177, 2000.

Sy, A., M. Rhein, J. R. N. Lazier, K. P. Koltermann, J. Meincke, A. Putzka, and M. Bersch, Surprisingly rapid spreading of newly formed intermediate waters across the Atlantic Ocean, *Nature, 386*, 675–679, 1997.

Weber, M. E., Estimation of biogenic carbonate and opal by continuous non-destructive measurements in deep-sea sediments from the eastern equatorial Pacific, *Deep Sea Res., Part I, 45*, 1955–1975, 1998.

Weber, M. E., F. Niessen, G. Kuhn, and M. Wiedicke, Calibration and application of marine sedimentary physical properties using a multi-sensor core logger, *Mar Geol, 136*, 151–172, 1997.

Wood, A. B., *A Textbook of Sound*, G. Bell, London, 1941.

A. E. Aksu and R. N. Hiscott, Earth Sciences Department, Memorial University of Newfoundland, St. John's, Newfoundland, A1B 3X5 Canada. (aaksu@sparky2.esd.mun.ca; rhiscott@sparky2.esd.mun.ca)

G. Bilodeau and C. Hillaire-Marcel, GEOTOP, Université du Quebec à Montréal, C.P. 8888, Montréal, H3C 3P8 Canada. (bilodeau.guy@uqam.ca)

L. A. Mayer, Center for Coastal and Ocean Mapping, University of New Hampshire, Jere Chase Ocean Engineering Bldg., Durham, NH 03824, USA. (lmayer@unh.edu)

F. Rack, Joint Oceanographic Institutions, Inc., 1755 Massachusetts Ave, NW, Suite 800, Washington, DC 20036, USA. (frack@brook.edu)

M. E. Weber, Ocean Mapping Group, Department of Geodesy and Geomatics Engineering, University of New Brunswick, P. O. Box 4400, Fredericton, New Brunswick, E3B 5A3 Canada. (mweber@unb.ca)

(Received June 30, 2000;
revised April 9, 2001;
accepted May 10, 2001.)